Processes of equatorial thermal structure at Jupiter: An analysis of the Galileo temperature profile with a three-dimensional model

T. Majeed,[1] J. H. Waite Jr., and S. W. Bougher
Space Physics Research Laboratory, University of Michigan, Ann Arbor, Michigan, USA

G. R. Gladstone
Southwest Research Institute, San Antonio, Texas, USA

Received 21 August 2004; revised 22 August 2005; accepted 7 September 2005; published 10 December 2005.

[1] The Jupiter Thermospheric General Circulation Model (JTGCM) calculates the global dynamical structure of Jupiter's thermosphere self-consistently with its global thermal structure and composition. The main heat source that drives the thermospheric flow is high-latitude Joule heating. A secondary source of heating is the auroral process of particle precipitation. Global simulations of Jovian thermospheric dynamics indicate strong neutral outflows from the auroral ovals with velocities up to ~1.2 km/s and subsequent convergence and downwelling at the Jovian equator. Such circulation is shown to be an important process for transporting significant amounts of auroral energy to equatorial latitudes and for regulating the global heat budget in a manner consistent with the high thermospheric temperatures observed by the Galileo probe. Adiabatic compression of the neutral atmosphere resulting from downward motion is an important source of equatorial heating from the top boundary of the JTGCM to 0.06 μbar. The adiabatic heating continues to dominate between 0.06 and 0.2 μbar, but with the addition of comparable heating due to horizontal advection induced by the meridional flow. Thermal conduction plays an important role in transporting heat down to lower altitudes (>0.2 μbar). The total heating transported in this region is radiated away by infrared hydrocarbon cooling via CH_4 (7.8 μm) and C_2H_2 (12.6 μm) emissions.

Citation: Majeed, T., J. H. Waite Jr., S. W. Bougher, and G. R. Gladstone (2005), Processes of equatorial thermal structure at Jupiter: An analysis of the Galileo temperature profile with a three-dimensional model, *J. Geophys. Res.*, *110*, E12007, doi:10.1029/2004JE002351.

1. Introduction

[2] On 8 December 1995 the Atmospheric Structure Instrument (ASI) on the Galileo probe provided the first in situ measurement of Jupiter's neutral atmospheric structure from 1029 km to 133 km (altitudes are referenced to a 1-bar pressure level) near the Jovian equator (Lat: 6.5°; λ_{III}: 4.5°) [*Sieff et al.*, 1998]. The derived temperature profile exhibited wave-like variations and increased from ~123 K at about 23 km (~0.36 bar) to ~900 K at 1027 km (~1 nbar), consistent with temperatures inferred from the solar (~10^{-5} μbar) and stellar (~1 μbar) occultation experiments performed during the Voyager flybys in 1979 [*Festou et al.*, 1981; *Atreya et al.*, 1981].

[3] H_3^+ emissions from the Jovian auroral and equatorial regions also provide information on the neutral temperature structure [*Drossart et al.*, 1989]. Analysis of such observations from the Canada-France-Hawaii Telescope (CFHT) by *Marten et al.* [1994] yielded an exospheric temperature of 800 ± 100 K near the Jovian equator. Spectral mapping of H_3^+ emissions from the Jovian upper atmosphere has also been obtained by Lam and coworkers [*Lam et al.*, 1997; *Miller et al.*, 1997] using the CGS4 spectrometer on the United Kingdom Infrared Telescope (UKIRT) on Mauna Kea. Information on the upper atmospheric temperatures and H_3^+ column densities derived from these observations indicate temperature variations near the Jovian equator. A temperature range from 750 K to 1000 K within ±10° latitude is derived which yields H_3^+ column densities of $(0.6-1.6) \times 10^{10}$ cm^{-2} (corresponding to an average pressure level of 1 nbar). *Hubbard et al.* [1995] observed the occultation of the star SAO 78505 by Jupiter at ~8° latitude and determined a temperature of 176 ± 12 K, in good agreement with the ASI temperature at a pressure level of 1.8 μbar. *Liu and Dalgarno* [1996] found an atmospheric temperature of 500 ± 30 K at 0.3 μbar for a best fit to the Hopkins Ultraviolet Telescope (HUT) day-

[1] Also at Department of Physics, American University of Sharjah, Sharjah, United Arab Emirates.

0148-0227/05/2004JE002351

Table 1. Summary of Observations

Date	Experiment	Payload	Latitude	Temperature, K	Pressure, bar	Reference
5 March 1979	solar occultation	Voyager 1	12.0°N	1100 ± 200	$\sim 10^{-11}$	*Atreya et al.* [1981]
9 July 1979	stellar occultation	Voyager 2	14.5°N	425 ± 25	$\sim 3 \times 10^{-10}$	*Festou et al.* [1981]
March 1992	spectroscopy	CFHT	10.0°N	800 ± 100	$\sim 10^{-11}$	*Marten et al.* [1994]
4 March 1995	UV dayglow	HUT	1.0°N	530 ± 70	$\sim 3 \times 10^{-7}$	*Liu and Dalgarno* [1996]
13 December 1989	stellar occultation	ground-based	8.0°N	176 ± 12	$\sim 2 \times 10^{-6}$	*Hubbard et al.* [1995]
8 December 1995	ASI probe	Galileo	6.5°N	123–900	-36–9.5×10^{-10}	*Sieff et al.* [1998]
1997	spectral imaging	UKIRT	global	875 ± 125	$\sim 10^{-9}$	*Miller et al.* [1997]

glow observation. This temperature is about a factor of two warmer than that observed by the Galileo probe at 0.3 μbar. Table 1 shows a summary of equatorial temperatures for Jupiter's upper atmosphere inferred from the above data sets.

[4] The observed temperature structure indicates that exospheric temperatures at Jupiter cannot be maintained by solar EUV heating alone [*Strobel and Smith*, 1973]. Dissipation of gravity waves [*Matcheva and Strobel*, 1999; *Young et al.*, 1997; *Yelle et al.*, 1996], soft and energetic particle precipitation [*Hunten and Dessler*, 1997; *Waite et al.*, 1997], and transport of auroral heat to low latitudes by thermospheric winds [e.g., *Waite et al.*, 1983] have all been proposed as mechanisms for heating the upper atmosphere.

2. Existing Interpretation of Galileo Temperature Profile

[5] *Young et al.* [1997] determined that the dissipation of upward-propagating internal gravity waves could produce enough heat to account for the high thermospheric temperatures measured by the Galileo probe. While *Matcheva and Strobel* [1999] and *Hickey et al.* [2000] argued that the propagation of gravity waves identified in the probe data can certainly heat the upper thermosphere, they proposed that the downward flux of sensible heat from the dissipating waves causes an appreciable cooling. Thus the net heating rate from the observed propagating gravity waves was insufficient to maintain the high Jovian thermospheric temperatures.

[6] Independently, *Waite et al.* [1997] modeled the energetics of Jupiter's upper atmosphere based on charged particles precipitating from the inner radiation belt to the Jovian equatorial atmosphere, resulting in X-ray emissions consistent with those observed by the high-resolution imager on the Rontgensatellit (ROSAT). The model calculations of altitude profiles of heating rates (∼150 times the solar EUV heating rate) suggested that the energy associated with the observed low-latitude X-ray brightness could be an important source of upper atmospheric heating and could account for Jupiter's high thermospheric temperatures. However, *Maurellis et al.* [2000] argued that a major fraction of the low-latitude Jovian X-ray emissions is due to the scattering and fluorescence of solar photons, and therefore cannot provide enough energy for the upper atmospheric heating. Recent X-ray observations of Jupiter with Chandra [*Gladstone et al.*, 2002] appear to support the scattered sunlight hypothesis, although there are some nonuniformities in the emission that could be indicative of charged-particle precipitation.

[7] The model calculations performed by *Sommeria et al.* [1995] have indicated that an extremely rapid auroral electrojet can generate supersonic neutral winds up to 20 km/s and could disperse high-latitude auroral heating globally through a strong meridional flow to explain high Jovian exospheric temperatures. However, there is no observational evidence to date for winds of such magnitude. The first three-dimensional (3-D) Jovian Ionospheric Model (JIM), developed by *Achilleos et al.* [1998], demonstrated that some of the energy deposited by high-latitude processes in the auroral regions can be transported to the Jovian equator by the meridional circulation of the neutral flow, yielding an equatorial temperature profile near local noon with an exospheric temperature of 1200 K [*Millward et al.*, 2002].

[8] Independently, we have developed a 3-D Jupiter Thermospheric General Circulation Model (JTGCM) to simulate the Jovian thermospheric winds self-consistently with global temperature and ion-neutral species distributions. An important goal of our model is to study the response of imposed high-latitude ion convection, along with particle and Joule heating, on the neutral flow, and its subsequent impact on the thermal structure. The details of the JTGCM, including the model inputs and global simulations of thermospheric dynamics and temperatures, have been recently reported by *Bougher et al.* [2005]. In this paper, we present the JTGCM analysis of the vertical thermal structure in comparison with that observed by the Galileo probe near the Jovian equator. We discuss heating and cooling processes within the equatorial region, which indicate that the transport of significant amounts of auroral energy by high-speed neutral winds can be sufficient to maintain the measured temperatures at the Galileo ASI probe location.

3. JTGCM

[9] The major characteristics of the JTGCM have been described by *Bougher et al.* [2005] in a comprehensive study of the thermospheric dynamics, energetics, and redistribution of thermospheric composition at Jupiter. In this paper, we briefly describe important points of the JTGCM that are related to this study.

[10] The JTGCM uses a 5° latitude by 5° longitude grid with 39 vertical pressure layers in increments of 0.5 pressure scale heights. The model solves coupled thermodynamic, zonal momentum, meridional momentum, continuity, and hydrostatic equations self-consistently using the basic framework of the National Center for Atmospheric Research (NCAR) general circulation model [cf. *Roble et al.*, 1988]. Each of these equations is cast in log-pressure coordinates ($Z_p = \ln(p_0/p)$), with a specified reference pressure level corresponding approximately to the average homopause level. For the JTGCM code, this reference

pressure is located at 4.5 μbar (Z_p = 0). Each Z_p interval corresponds to a 1-scale height (at the local temperature).

3.1. Boundary Conditions

[11] The lower boundary in the JTGCM is at 20 μbar, to take into account the hydrocarbon cooling due to C_2H_2 (12.6 μm) and CH_4 (7.8 μm) at the base of the thermosphere, below the homopause [*Drossart et al.*, 1993]. In particular, this is important for proper cooling of the Jovian auroral atmosphere where strong electron precipitation provides heating that is conducted downward and radiated away via these strong infrared (IR) emissions. H_3^+ cooling from IR emissions [*Drossart et al.*, 1989] has also been included above the homopause. Our assumed boundary conditions are that the geopotential, zonal, and meridional winds are zero at the lower boundary (i.e., strict corotation). This is certainly a crude simplification that neglects the strong stratospheric winds [e.g., *Flaser et al.*, 2004] and upward propagating tides and gravity waves [e.g., *Young et al.*, 1997, 2005; *Matcheva and Strobel*, 1999; *Hickey et al.*, 2000] that must be present in the Jovian lower atmosphere. Global average lower boundary conditions both for the temperature and neutral densities (H and He) are taken from Galileo [*Sieff et al.*, 1998] and Voyager data [*Festou et al.*, 1981]. Specifically, an average global temperature, composed of observed equatorial and polar values near 250 km, is set to 190 K. The helium volume mixing ratio is set to 0.135 at 250 km, based upon Galileo probe observations [*Niemann et al.*, 1996]. The atomic hydrogen volume mixing ratio is set to 4.23×10^{-8}, in accord with Voyager data. Photochemical equilibrium is assumed for the major ions (H_2^+ and H_3^+).

[12] Upper boundary conditions were specified at $\sim 1.1 \times 10^{-4}$ nbar in order to properly include high-altitude auroral heating processes [*Ajello et al.*, 2001; *Grodent et al.*, 2001] and H_3^+ cooling in the near-IR [*Drossart et al.*, 1989]. Corresponding boundary conditions for temperatures and neutral winds are identical to those employed in the terrestrial TIGCM; vertical gradients in temperatures and winds (zonal, meridional, and vertical) are set to zero at the top of the model. These conditions are in accord with weak energy sources at high altitudes; isothermal temperatures are also consistent with the emergence of the exosphere. For composition (H and H_e), diffusive equilibrium is assumed at the top boundary [cf. *Bougher et al.*, 2005].

[13] Each of the JTGCM equations is time dependent, but is typically integrated toward steady state conditions. Thus the JTGCM simulations of the thermosphere/ionosphere code are conducted for many Jovian rotations in order to approach a cyclic steady state solution in the modeled fields. Planetary TGCMs achieve steady state solutions according to various timescales that vary as a function of altitude [e.g., *Bougher et al.*, 1999]. For Jupiter's thermosphere, a dynamical timescale can be defined as the transport time for average meridional winds to redistribute auroral oval heating and atomic species to the jovigraphic equator. Typical JTGCM zonally averaged meridional winds ($\sim$125–300 m/s) [*Bougher et al.*, 2005] place this timescale at about 4 to 10 Earth days for pressures below about 0.15 μbar. Equilibration requires that meridional pressure gradients are stabilized by both pole-to-equator and equator-to-pole wind flow, for which the dynamical timescales should be multiplied by 2. This yields an effective dynamical timescale of the order of 8–20 Earth days (or 20–50 Jovian rotations). Hence JTGCM calculations can only achieve near equilibrium solutions for the upper thermosphere when simulations run on the order of $\geq$50 Jovian rotations. Further discussion on the JTGCM computational scheme, numerical stability, filtering and smoothing of prognostic fields has been published recently by *Bougher et al.* [2005].

3.2. Input Parameters

[14] The JTGCM uses solar EUV radiation as a source of equatorial heating, while the particle heating calculated by *Grodent et al.* [2001] (incident electron energy spectrum described by a combination of three Maxwellian distribution functions with total particle energy $E_\circ$ = 25 keV and energy flux $\sim$110 ergs cm^{-2} s^{-1}) is used for the auroral region. An average solar EUV heating rate profile estimated by *Waite et al.* [1983] is specified within the latitude band of ±50° latitude to investigate the relative importance of this heating mechanism on the Jovian equatorial thermosphere. The auroral heating by particle precipitation is specified symmetrically in λ_{III} longitude along both the northern and southern polar ovals, which are currently described by the auroral morphology deduced from analysis of WFPC2 images taken in 1996 and 1997 [*Clarke et al.*, 1998]. Recent analysis of HST-STIS images by *Grodent et al.* [2003] indicates that the auroral oval locations on Jupiter are constant in latitude and system III longitude. In addition, Joule heating, which is driven by the differential velocity between the ion and neutral species in the auroral ionosphere, has also been described in the JTGCM code as an important mechanism for modifying Jupiter's global thermospheric winds and temperatures. The treatment of Joule heating in the JTGCM is described later.

[15] An important parameter of the JTGCM is the high-latitude ion drift around the auroral ovals resulting from the magnetic coupling between an equatorial plasma sheet within the middle magnetosphere and the Jovian upper atmosphere. The main auroral ovals have now been linked to the breakdown of plasma sheet corotation at 20–30 R_j, where large field-aligned currents are generated by the transfer of Jupiter's angular momentum to Iogenic plasma that is being driven centrifugally outward [*Hill*, 2001]. This process results in the precipitation of energetic electrons, causing ionization and heating of the neutral gas. Thus the main ovals are the dominant source of much of the auroral ionization yielding a highly conducting ionosphere, and are the likely origin of fast-ion drifts in Jupiter's ionosphere: the auroral electrojet [e.g., *Cowley and Bunce*, 2001]. In the current version of the JTGCM, we use an estimated convection electric field and corresponding ion drifts (u_i and v_i) from a simplified ionospheric convection model as inputs. Such estimates are based on Voyager measurements of ion convection in the outer magnetosphere [cf. *Eviatar and Barbosa*, 1984] mapped to high latitudes using the VIP4 magnetic field model [*Connerney et al.*, 1998]. In this manner, anti-corotational electrojet winds up to 3.0 km/s (see *Bougher et al.* [2005] for details) are estimated and prescribed around both main auroral ovals, driving the neutral winds to move in the same direction. Conversely, in nonauroral regions, u_i and v_i are zero (i.e., corotational);

corresponding neutral winds are decelerated by ion-drag forcing in those regions where the ion-neutral collision frequency remains high.

[16] Ion-drag within the JTGCM code is described as a dominant physical process, which limits neutral wind speeds through couplings between ions in the Jovian auroral ovals and the corotating neutral atmosphere. The ions, magnetically connected to the subrotating regions of the magnetosphere, lose their momentum in collisions with neutrals and thus drive the neutrals to move in roughly the same direction. Thus in the auroral region, this drag is proportional to the product of the ion density (mostly H_3^+) and the relative drift between the neutral and ion constituents. The density of H_3^+ in the JTGCM is calculated by assuming photochemical equilibrium owing to its short lifetime ($<10^3$ s). A parameterized production function of H_2^+ [*Waite et al.*, 1983] is assumed to be the dominant source, while dissociative recombination is considered the major sink for the H_3^+ ion. The H^+ ion is presently prescribed within the JTGCM on the basis of a detailed 1-D profile calculated offline [*Waite et al.*, 1983] throughout the Jovian globe. It is well known that the ionosphere is largely controlled by H^+ production above an altitude of 1200 km and by H_3^+ below this altitude, regardless of the presence of winds and energetic particle precipitation [*Majeed et al.*, 1999; *Maurellis and Cravens*, 2001]. Current interpretations of the measured vertical ionospheric structure indicate that a combination of vertical plasma drift and enhanced populations of vibrationally excited H_2 molecules with $v \geq 4$ is required in 1-D models [*Majeed et al.*, 2004]. Thus a proper calculation of H^+ densities requires a loss mechanism involving H_2 vibrational levels [*Cravens*, 1987; *Majeed and McConnell*, 1991]. However, this key loss for H^+ was not properly treated within the Waite et al. 1-D model, and likewise is ignored in the present JTGCM code. The proper calculation of these H_2 vibrational levels in a future version of the JTGCM code will allow us to simulate a realistic upper ionosphere self-consistently with the Jovian thermal and dynamical structures on a global basis.

[17] Ion-drag is a dominant neutral momentum forcing process at auroral oval latitudes near the altitude of the ionospheric peak. At greater ionospheric heights the effect of ion-drag gradually decreases as the ion gyrofrequency exceeds the ion-neutral collision frequency that constraints ionization to move along magnetic field lines. *Richmond et al.* [1992] have shown that ion-drag can significantly modify the neutral winds at Earth's low and mid latitudes, thereby affecting the distribution of neutral temperatures.

[18] The parametrization of ion-drag and Joule heating in the JTGCM code is based on the formulation described by *Roble and Ridley* [1987]. Recently, *Bougher et al.* [2005] demonstrated that scaling of ion-drag and Joule heating rates may be needed to explore general characteristics of the global structure and dynamics, which can be used to explain multispectral observations of the Jovian thermosphere. This scaling may reflect uncertainties in the (1) magnetosphere-ionosphere mapping that we have conducted using the VIP4 magnetic field model [*Connerney et al.*, 1998] and (2) derived high-latitude ion convection [*Eviatar and Barbosa*, 1984] from Voyager observations of the middle magnetosphere of Jupiter. This is not too surprising since early versions of the Earth's TGCM, allowed Joule heating rates to vary as much as a factor of 20 from the global heating estimates based on derived time-mean currents in the dynamo region [*Matsushita et al.*, 1973]. The global simulations from these models were utilized to interpret thermospheric temperatures and radar observations of neutral winds at low and mid latitudes [*Dickinson et al.*, 1975]. Joule heating in current models (e.g., TIEGCM) is induced by high-latitude plasma drifts associated with magnetospheric convection driven by a cross-tail potential that is highly variable, ranging from 20 kV to perhaps 200 kV depending on geomagnetic conditions [*Roble and Ridley*, 1994]. Thus, for the terrestrial thermosphere, this is an important parameter to account for diurnal neutral temperature distribution and thermospheric circulation. Similarly, variations in Joule heating are equally important in modifying the global thermospheric circulation on Jupiter.

[19] Our estimates of hydrocarbon cooling due to strong C_2H_2 (12.6 μm) and CH_4 (7.8 μm) radiation in the JTGCM are based on constraints provided by re-analyzing the Voyager 1 infrared Interferometer and Radiometer Spectrometer (IRIS) spectra [*Drossart et al.*, 1993]. Note that the infrared cooling resulting from C_2H_6 emission is negligible in our JTGCM domain, and is therefore neglected. The total measured excess infrared auroral zone emission (averaged over the IRIS field of view) in the hydrocarbon bands between 7 and 13 μm was found to be about 208 erg cm^{-2} s^{-1} over an area of about 2×10^{18} cm^2 with a resulting power output of 4×10^{13} W. This large infrared output likely results from a large temperature enhancement in the upper stratosphere and lower thermosphere, in accord with strong auroral and Joule heating that is conducted downward and made available for infrared radiation [*Bougher et al.*, 2005].

[20] Most recently, *Yelle et al.* [2001] reevaluated radiative processes in Jupiter's stratosphere between 0.1 bar and 10^{-6} bar based on constraints provided by the Galileo temperature profile and composition profiles derived from various experiments. Heating and cooling rates were calculated based on realistic altitude profiles of C_2H_2, C_2H_6, and CH_4 profiles which are in reasonably good agreement with predictions from photochemical models [e.g., *Gladstone et al.*, 1996]. Interestingly, *Yelle et al.* [2001] predicted that absorption of solar radiation in CH_4 bands is the dominant heat source in the equatorial Jovian stratosphere. The 3.3 μm band is the primary heat source at pressures less than 4×10^{-6} bar, while the 2.3 μm band dominates the heat budget between 4×10^{-6} and 5×10^{-4} bar. Another important conclusion of Yelle et al.'s model is the dominance of C_2H_6 cooling throughout the stratosphere with a minor contribution from C_2H_2, contrary to many earlier studies [e.g., *Grodent et al.*, 2001]. As noted above, the current version of the JTGCM code does not include these heating and C_2H_6 cooling terms. However, future upgrades to the JTGCM code will incorporate Yelle et al.'s model to improve the self-consistency of the energetic, dynamical, and chemical processes at lower thermospheric altitudes (>1 μbar).

4. Results and Discussion

4.1. Temperature Simulation

[21] Using the current version of the JTGCM, we have demonstrated that the underlying global thermospheric

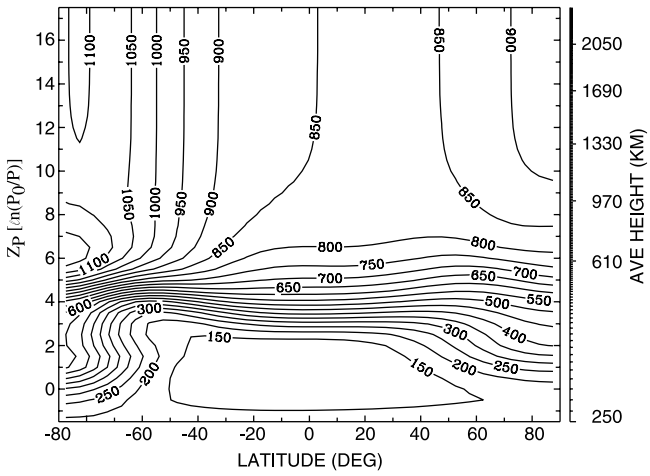

Figure 1. JTGCM contours of zonally averaged temperatures are shown for the simulation which best describes the measured thermal structure at the entry location of the Galileo probe. Note that the reference pressure level (p_0) is 4.5 μbar.

circulation is greatly intensified when ion drag and Joule heating processes are applied to an otherwise aurorally particle precipitation driven wind system. The resulting strong neutral winds play a significant role in redistributing high-latitude heat and neutral composition toward the equator. Recently, *Bougher et al.* [2005] have shown that scaling of ion-drag and corresponding Joule heating by adjusting the horizontal ion drift implemented in the JTGCM has an important influence on the global thermospheric structure and circulation. They have suggested a downward scaling of this drift by 30% for the JTGCM simulations for analyzing observations of the Jovian thermosphere. It is important to note we used a different scaling method than that adopted by *Bougher et al.* [2005]. Rather than adjusting ion drifts, we scale the total Joule heating produced in the Jovian auroral ovals by a factor that could reproduce equatorial thermal structure observed by the Galileo probe. Regardless of which method is to be used, the required adjustment in Joule heating is quite reasonable and in accord with early versions of the terrestrial TCGM [cf. *Dickinson et al.*, 1975].

[22] Figure 1 shows one of the simulations of zonally averaged temperatures with the best case scenario, which includes an auroral forcing by particle heating and an additional forcing by 15% of the total Joule heating produced in the auroral ovals. The simulation was run for 82 Jovian rotations to achieve steady state temperature and wind fields for pressures >1 μbar, while at higher pressures the JTGCM fields remain to be stabilized. Note that the neutral temperature is quite uniformly distributed globally for lower thermospheric heights with pressure >30 nbar (or zp < 5) with the exception of the high-latitude region near the southern pole (70–90°S). A north-south asymmetry also exists in the temperature distribution, which is consistent with that observed in the H_3^+ temperature map derived from spectral imaging of the Jovian atmosphere [*Miller et al.*, 1997]. Such a distinct behavior of the global temperature seems to reflect strong ion-drag forcing due to the magnitude of zonally averaged ion winds (u_i) in the southern auroral oval, which is about a factor of 2 larger than in the northern auroral oval [e.g., *Bougher et al.*, 2005]. In addition, the local topology of the VIP4 magnetic field in the Northern Hemisphere is quite different from that in the southern Hemisphere [cf. *Connerney et al.*, 1998]. For the simulated JTGCM electron densities, calculated Pedersen conductivities are generally larger in the Southern Hemisphere compared to those in the Northern Hemisphere [*Bougher et al.*, 2005]. Thus ion-drag, together with Joule heating, effectively enhance momentum transfer in the global circulation affecting the neutral winds and temperatures.

[23] In the upper thermospheric regions (pressure $\leq$ 30 nbar or zp $\geq$ 5), horizontal winds up to 1.2 km/s, driven largely by additional Joule heating, appear to be responsible for creating strong upwelling and divergence of the neutral flow in the polar regions, while convergence and subsidence of this flow is seen at the Jovian equator. Such a global circulation of neutral flow results in an increase in neutral temperatures throughout the thermosphere compared to simulated temperatures with particle heating alone (see section 4.2). Joule heating dominates heat budgets in both hemispheres [e.g., *Bougher et al.*, 2005], yielding exospheric temperatures of 900–1100 K in the auroral regions, consistent with UKIRT [*Miller et al.*, 1997] and CFHT [*Raynaud et al.*, 2004] multispectral observations, while the temperature near the Jovian equator is ~890 K (see Figure 1). The details of equatorial thermal balance for this simulation will be discussed in section 4.3.

4.2. Comparison With Temperature Data

[24] In Figure 2 we compare the JTGCM temperature profiles, simulated at the entry location of the Galileo probe, with the measured (Curve A) and modeled thermal structures from various sources listed in Table 1. Curve B is the JTGCM fit to the measured temperature profile, Curve A, from the simulation which incorporates ion-drag and moderate auroral heating caused by precipitated charged particles combined with solar EUV heating around the Jovian equator. This simulation, which ignored Joule heating, ran for 80 Jovian rotations to achieve steady state conditions at pressures below the 1 μbar level. The gradual cooling of the high-latitude auroral thermosphere has been seen in response to local pressure gradients that drive neutral winds (of the order of 1 km/s) away from the heated regions. These winds serve to reduce auroral temperatures in the exospheric region from 1000 K at the start of the simulation to around 600–700 K at the end of the simulation. At the Jovian equator, an exospheric temperature as high as 475 K (Curve B) is obtained. This temperature is more than a factor of two warmer than what would have resulted from a simulation relied only on solar inputs to heat the atmosphere [*Strobel and Smith*, 1973]. However, it is also shown that the simulated temperature is about a factor of 2 cooler than the actual temperature measured by the Galileo ASI instrument (Curve A). Clearly, this difference in temperatures indicates that heat has been transported from auroral regions to the equatorial region by a strong meridional flow. Molecular thermal conduction acts to direct this heat downward toward the CH_4 homopause where the hydrocarbon cooling, primarily

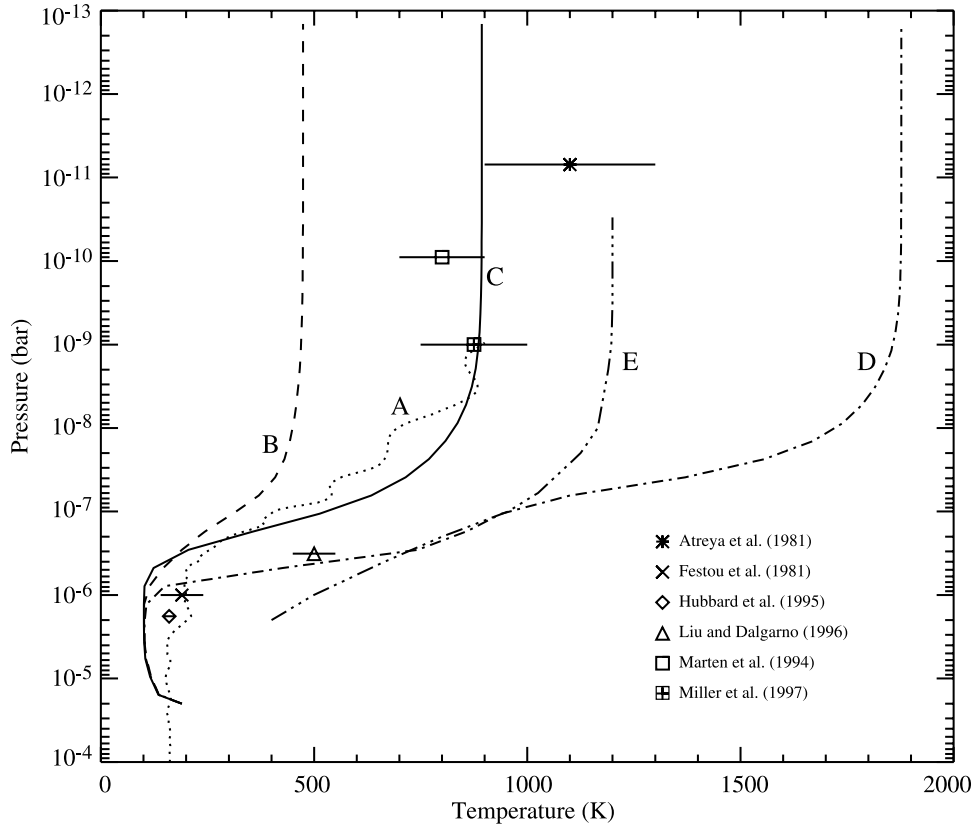

Figure 2. JTGCM temperature profiles are shown in comparison with the equatorial temperature profiles from JIM (Curve E) and in situ measurements by the Galileo ASI probe (Curve A). Remotely sensed temperature observations from various sources are also compared with the simulated temperatures. Curve B is from simplified simulation (ion-drag, high-latitude auroral heating, and solar EUV heating). Curve C is from a simulation that incorporates 15% of the total Joule heating produced in auroral ovals plus Curve B conditions. Curve D is from a simulation that assumes 30% of the total Joule heating plus Curve B conditions.

caused by CH_4 (7.8 μm) and C_2H_2 (12.6 μm) emissions, rapidly radiates this heat away. By examining the JTGCM heating terms, it is evident that the transported heat at the ASI probe location corresponding to Curve B is not sufficient to explain the measured characteristics of the Jovian thermal structure. Clearly, an additional heat source in the JTGCM is required to reproduce the observed temperature profile.

[25] Curve C shows a reasonable fit to the Galileo temperature profile by assuming 15% of the total Joule heating produced in auroral ovals in addition to charged-particle heating and the equatorial EUV heating. This simulation is run for 82 Jovian rotations by using the previous simulation (Curve B) as initial conditions. Again, a steady state solution to the JTGCM fields is obtained up to 1 μbar, while oscillations in these fields for pressures greater than 1 μbar remain to be stabilized. The JTGCM temperatures at 0.1 and 0.01 nbar are also found to be in reasonably good agreement with those inferred from the analysis of CFHT high-resolution H_3^+ emission spectra [*Marten et al.*, 1994] and Voyager UVS solar occultation data [*Atreya et al.*, 1981], respectively. However, the model temperatures in the stratospheric region (between 1 and 2 μbar) appear to be slightly cooler than the measured temperatures.

[26] A comparison of the isothermal layer of ~100 K between 1 and 10 μbar, simulated by the JTGCM, is found to be considerably cooler than the temperature structure measured by the Galileo probe. Apparently, for this simulation, which incorporates Joule heating in the auroral ovals, meridional flow of heat transport is still insufficient to compete with radiative and adiabatic processes of cooling. Thus the thermal budget at the entry location of the Galileo probe is dominated and controlled by the resulting net cooling from hydrocarbon (CH_4 and C_2H_2) radiation and upwelling winds. Recall that the heating rate resulting from absorption of sunlight in the CH_4 bands at 3.3 μm is not presently incorporated in the JTGCM code. The altitude profile of such a heating rate has been calculated by *Yelle et al.* [2001] at the Galileo probe location. Note that the magnitude of CH_4 heating rates from 1 μbar to the lower boundary of the JTGCM (20 μbar) are in the range 9.8×10^4 to 5.3×10^5 eV cm^{-3} s^{-1}, compared to the JTGCM heating rates of 2×10^5 to 6.2×10^6 eV cm^{-3} s^{-1} (see section 4.5 for details). The use of CH_4 heating in the JTGCM will impact the equatorial thermal budget and probably enhance the temperature of the isothermal layer in the upper stratospheric region.

[27] In the region between 1 and 0.01 μbar, the JTGCM (curve C) predicts rapidly rising temperatures as the merid-

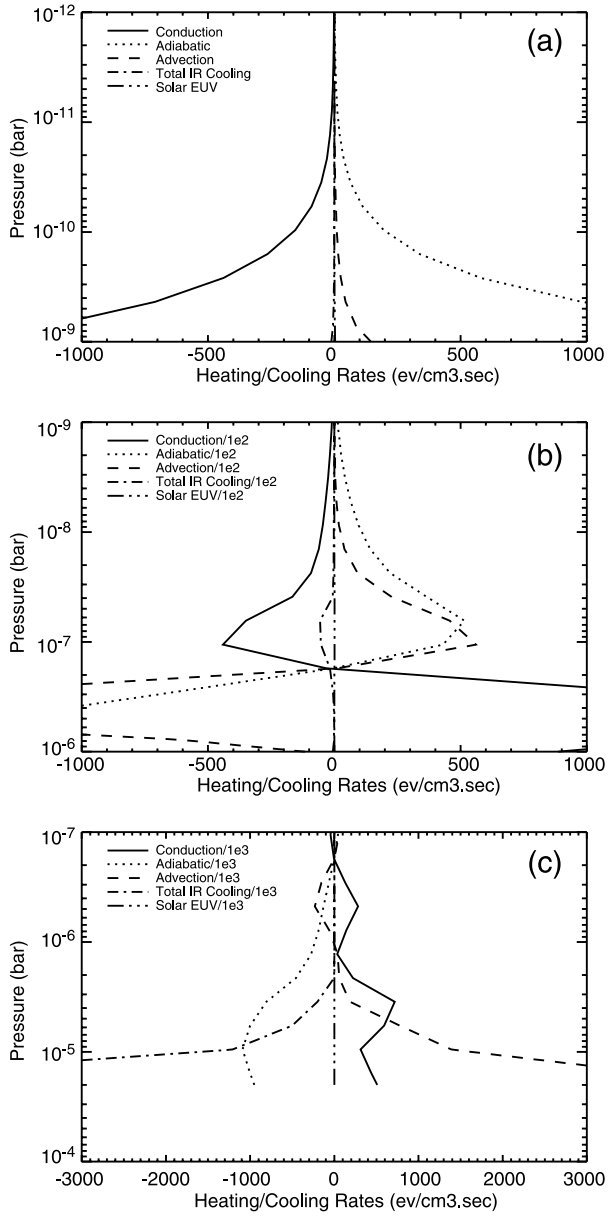

Figure 3. Altitude profiles of heating and cooling rates are shown for the JTGCM simulation representing Curve C in Figure 2 for three pressure regions, (a) 10^{-9} to 10^{-12} bar, (b) 10^{-6} to 10^{-9} bar, and (c) 10^{-4} to 10^{-7} bar. Note that the heating and cooling rates are scaled in Figures 3a, 3b, and 3c, by 1, 10^{-2}, and 10^{-3}, respectively.

ional flow of auroral winds carries auroral energy to lower latitudes. A similar rapid rise can be seen in the measured temperature, which has large vertical temperature gradients with a peak value of ~3 K/km at 0.3 μbar [cf. *Sieff et al.*, 1998]. However, our model (curve C) predicts a peak value of about 5 K/km at 0.3 μbar in the altitude profile of the temperature gradient. At the ASI probe location, our model also predicts an integrated energy flux of ~1.35 ergs cm^{-2} s^{-1} for the region with pressures <1 μbar, for which the JTGCM has achieved steady state conditions (see section 4.3 for details). The energy flux in this region is primarily from adiabatic compression of the neutral atmosphere and meridional transport of heat from the auroral ovals. The predicted value of energy flux is almost 30% larger than that used analytically by *Yelle et al.* [1996] to explain the measured temperatures at 10 nbar [*Marten et al.*, 1994] and 0.3 μbar [*Liu and Dalgarno*, 1996] by assuming energy from dissipating gravity waves alone. Clearly, dynamical sources of heat play an important role in our understanding of the bulk of the equatorial heat budget for the region where steady state conditions prevail. However, as the pressure increases toward the lower boundary, the JTGCM fields begin to oscillate, causing a departure of the temperature fields from steady state conditions. The dynamical heating in this region with strong thermospheric winds is efficiently dissipated by hydrocarbon cooling, caused by CH_4 (7.8 μm) and C_2H_2 (12.6 μm) radiation [*Bougher et al.*, 2005].

[28] The effects of excess Joule heating on the heat transport processes, which control the thermospheric temperatures in the auroral [c.f. *Bougher et al.*, 2005] and equatorial regions, have also been studied. Curve D shows an example of the equatorial temperature profile from the simulation which assumes twice the Joule heating (30%) compared to the one which explains the Galileo temperature profile. In this case, the exospheric temperature reaches up to 1880 K as a result of increased meridional transport of auroral heat to the entry location of the Galileo probe.

[29] Figure 2 also shows a comparison between the equatorial temperature profiles derived from the JIM (Curve E) and JTGCM simulations. While the energy transport from auroral ovals down to the equatorial region by horizontal neutral winds has been demonstrated by both models, the JIM simulation has shown warmer thermospheric temperatures up to 300–500 K [e.g., *Millward et al.*, 2002] compared to those simulated by the JTGCM (Curve C). Perhaps, the possible explanation of such a large temperature difference between the two models appears to be due to transport processes and/or due to the absence of hydrocarbon and H_3^+ radiative cooling in JIM. On the other hand, *Bougher et al.* [2005] have recently noted that cooling associated with upward neutral motion and local H_3^+ radiation is required to regulate dynamical heat transported from auroral ovals to control the equatorial thermal budget and to maintain warm thermospheric temperatures. While a dynamical timescale in excess of 50 Jovian days is required to obtain a balance between cooling and heating rates, it is not possible for JIM to obtain such a balance because it has been integrated only for a few Jovian days. Clearly, the simulated profile from JIM (Curve E) shows a rapid increase in temperature from 400 K at the lower boundary (2 μbar) to about 1200 K at exospheric heights.

4.3. Equatorial Thermal Balance

[30] In Figure 3 we show the vertical profiles of transport sources for thermospheric heating and cooling from the JTGCM simulation, which best describes the thermal structure measured in situ by the Galileo probe (curve C of Figure 2). Note that the contributing solar EUV energy source for the upper thermospheric heating is negligibly small, but is included in the model for completeness. Figure 3a illustrates the balance between adiabatic heating, caused by the downward flow of the neutral atmosphere, and cooling by thermal conduction. Certainly, this balance

Table 2. Heating and Cooling Timescales at Various Pressure Levels

Pressure, μb	Cp, erg K^{-1} g^{-1}	ρ, g cm^{-3}	$Q_T^{H,a}$ erg cm^{-3} s^{-1}	$Q_T^{c,b}$ erg cm^{-3} s^{-1}	T, K	τ_H, s	τ_c, s
16	1.30×10^8	3.14×10^{-9}	4.23×10^6	6.54×10^6	117	7.10×10^6	4.60×10^6
0.5	1.37×10^8	5.22×10^{-11}	2.46×10^5	2.17×10^5	124	2.24×10^6	2.31×10^6
0.06	1.41×10^8	2.36×10^{-12}	9.70×10^4	4.80×10^4	635	1.35×10^6	2.70×10^6
10^{-3}	1.45×10^8	3.07×10^{-14}	1.73×10^3	1.23×10^3	885	1.40×10^6	1.80×10^6

[a] Q_T^H, total heating rate.
[b] Q_T^c, total cooling rate.

plays an important role in maintaining an exospheric temperature of ~890 K, consistent with the observed temperature. The smooth equatorial temperature profile in this region is consistent with the fact that conduction dominates all other sources of cooling. In the region between 0.2 μbar and 1 nbar, the Jovian wind system seems to play an active role in transporting energy from the auroral region to the equatorial region. Figure 3b shows that the adiabatic process continues to dominate the heat budget, with a peak value of $\sim 5 \times 10^4$ eV cm^{-3} s^{-1} at 0.06 μbar. While horizontal advection, induced by meridional flow with a maximum velocity of ~55 m/s [*Bougher et al.*, 2005], becomes an important source of heating at 0.1 μbar ($\sim 5.5 \times 10^4$ eV cm^{-3} s^{-1}), the process of heat conduction combined with the H_3^+ cooling tends to cool down the atmosphere up to a pressure level of 0.2 μbar, with a maximum cooling rate of $\sim 5 \times 10^4$ eV cm^{-3} s^{-1} calculated at around 0.1 μbar. Thus the net heating rate is overwhelmed by transport sources, yielding a rapid increase in equatorial temperatures between 0.2 μbar and 0.01 μbar (see Figure 2).

[31] Figure 3c reveals the importance of vertical energy transport by thermal conduction in the Jovian thermosphere from 1 to 0.2 μbar. The maximum heating rate from the conduction process is about 2.5×10^5 eV cm^{-3} s^{-1} at around 0.5 μbar, which is primarily balanced by the cooling associated with wind transport processes. Jupiter's thermosphere from 1 μbar to the lower boundary of the JTGCM is the most complicated region. The competing processes responsible for controlling the thermal structure have not yet reached equilibrium. Upward motion is still causing atmospheric expansion while meridional flow is still transporting heat from auroral regions. The net heating rate for the thermal structure in this region is determined by the competition between heat transport processes and radiative cooling processes. Although, strong cooling associated with upwelling winds appears to be in balance with strong dynamical heating caused by meridional flow, an effective sink for transported heat is provided by an extremely large amount of cooling resulting from CH_4 (7.8 μm) and C_2H_2 (13.4 μm) radiation. The effect of such a large cooling rate on the simulated thermal structure has been shown by cooler temperatures (Curve C in Figure 2) compared to those inferred from the ASI probe, and Voyager [*Festou et al.*, 1981] and groundbase stellar occultation [*Hubbard et al.*, 1995] experiments.

4.4. Timescales

[32] The simulated thermal processes shown in Figure 3, which best describe the thermal structure derived from the ASI probe data, are used to estimate timescales of heating and cooling for the Jovian thermosphere. This will allow us to investigate long-term effects of energy transport and deposition on the distribution of the neutral temperature. Table 2 shows the estimated timescales of heat transport and the corresponding timescales of cooling at four different pressures from $\tau = c_p \rho T / Q_T$, where Q_T is the total heating/cooling rate from all sources, while T is the neutral temperature. c_p and ρ are specific heat and atmospheric density appropriate for an H_2 atmosphere, respectively. It is important to note that the simulated heating and cooling rates reach their maximum values at these pressures (see Figure 3). Thus the timescale magnitude at each pressure is the key to test the ability of the JTGCM to achieve long-term stability in the neutral temperature and wind fields.

[33] The timescales of heat transport at 1 nbar and 0.5 μbar are estimated to be 1.4×10^6 s and 2.2×10^6 s, respectively. These timescales are quite comparable to the corresponding timescales of cooling. At 0.06 μbar, however, the timescale of cooling is about a factor of 2 longer than the corresponding heating timescale. Clearly, at 1 nbar and 0.5 μbar, the magnitudes of heating and cooling timescales suggest that an estimated time of ~40–66 Jupiter's days is required for the Jovian winds to transport auroral heat to the equatorial region (Galileo probe location) and to cool off the upper thermosphere. However, at 0.06 μbar, the estimated time for the JTGCM to cool down the transported heat exceeds 78 Jupiter's days. This longer cooling timescale suggests that the energy transport by meridional flow, with a speed roughly estimated as $R_j/\tau_c \sim 27$ m/s (R_j being Jupiter's radius) [*Bougher et al.*, 2005], should not be lost to downward conduction along the way to the Jovian equator. Note that the recent analytical study of the equatorial thermal structure of Jupiter by *Yelle and Miller* [2004] showed an estimated cooling timescale of $\sim 4 \times 10^6$ s by assuming H_3^+ radiation alone at 0.01 μbar. This value is in excellent agreement with the corresponding timescale of 2.3×10^6 s from the JTGCM simulation which shows that conduction dominates all the other cooling terms at 0.01 μbar (see Figure 3).

[34] An interesting situation occurs at 16 μbar, near the lower boundary of the JTGCM. At this particular pressure, the magnitude of cooling timescale is estimated to be ~35% less than the corresponding heating timescale (Table 2). Recall that in the region with pressures >1 μbar, the cooling resulting from heat dissipation dominates and controls the equatorial temperature structure (Figure 2). Thus it appears that a strong meridional flow is still required to transport high-latitude auroral heat and Joule heat to compensate for such a large cooling in the JTGCM simulation (Curve C of Figure 2) which predicts an average meridional wind of ~10 m/s. Because the global circulation of the neutral flow is affected by Coriolis force, it is important to investigate what magnitude of mean meridional winds is needed to

Table 3. Column-Integrated Thermal Balances[a]

Process	Pressure			
	20 μbar to1.4 nbar	>1 μbar	<1 μbar	<1 nbar
Conduction	3.35	4.14	−0.98	−0.058
Adiabatic	−4.79	−7.98	0.53	0.061
Advection	14.83	12.69	0.82	0.0033
Total IR cooling	−30.46	−16.96	−0.12	-1.88×10^{-4}
Equatorial EUV	0.004	0.004	0.004	9.04×10^{-5}
Total heating	18.18	16.83	1.35	0.064
Total cooling	35.25	24.94	1.10	0.058

[a]Units are erg cm^{-2} s^{-1}.

overcome Coriolis effects. One way to find this out is to continue the present simulation for many more planetary rotations. This would allow us to study whether Coriolis force tends to turn meridional winds in a zonal direction or these winds grow in magnitude. An alternative to this approach is to use realistic lower boundary conditions in the JTGCM from high-pressure dynamical models such as the one developed by *Conrath et al.* [1990] (see also *Moses et al.* [2004] for references).

4.5. Integrated Thermal Balances

[35] The total heating simulated at the Galileo probe location by the JTGCM should be reflected in the corresponding total cooling that results from its dissipation. In Table 3, we summarize the calculated column-integrated heating and cooling rates from the thermal processes (see Figure 3) which compete to control the bulk of the thermal budget and to maintain the warm equatorial temperatures observed by the Galileo probe. Note that these rates are calculated and represented in ergs cm^{-2} s^{-1}.

[36] An extremely large heating rate (up to 18.18 ergs cm^{-2} s^{-1}) is determined for the entire thermospheric region from 1.4 nbar to 20 μbar. Horizontal advection appears to be the main contributor to this integrated heating, which reflects the enhanced role of intensified meridional circulation in the Jovian thermosphere. However, a small fraction of the total integrated heating is provided by the conduction process. The total cooling is dominated by the column-integrated rate of IR cooling (almost 89%), mainly from CH_4 (7.8 μm) emission [cf. *Yelle et al.*, 2001], with a small contribution from adiabatic cooling (about 11%). The bulk of this strong IR cooling serves to balance the strong dynamical heating and tends to remain in control of the equatorial thermal budget. Note that a major portion of the intense column heating is produced near the lower boundary of the JTGCM (>5 μbar; see Figure 3) which is mainly regulated by an intense column of hydrocarbon cooling.

[37] The integrated heating and cooling rates for pressures >1 μbar have also been calculated to demonstrate how equatorial processes are used to interpret the thermal structure in this region of the Jovian thermosphere. Clearly, hydrodynamic advection (12.69 ergs cm^{-2} s^{-1}) dominates the heat budget while hydrocarbon IR cooling (16.96 ergs cm^{-2} s^{-1}) radiates this heat away. The resulting net cooling of about 8 ergs cm^{-2} s^{-1} explains the much cooler isothermal layer between 1 and 10 μbar simulated by the JTGCM (see Figure 2). This also suggests that steady state conditions in the JTGCM have not been achieved for pressures >1 μbar.

[38] Table 3 also shows the column-integrated heating and cooling rates for the upper thermospheric regions (<1 μbar) for which the steady state conditions for temperature and wind fields prevail. The column heating rates for the region with pressures less than 1 μbar and 1 nbar, resulting from adiabatic process and hydrodynamic advection associated with strong meridional and subsiding flow, are reaching the maximum value of 1.35 ergs cm^{-2} s^{-1} and 0.064 ergs cm^{-2} s^{-1}, respectively. Downward conduction and H_3^+ (2–4 μm) radiation provide the necessary column of integrated cooling to balance the dynamical heat to interpret the Galileo ASI temperature profile.

5. Summary

[39] The global dynamical structure of the Jovian thermosphere is simulated self–consistently with thermal structure and composition distributions using a three-dimensional Jupiter Thermosphere General Circulation Model (JTGCM). We have shown that the global circulation of the neutral wind system, driven by auroral heating and 15% of the total Joule heating produced in the auroral ovals, can transport sufficient energy near the Jovian equator to explain the thermal structure observed by the Galileo probe. The energy transport processes associated with the Jovian wind system play a significant role in the global distribution of neutral temperatures. The cooling of auroral regions is caused by strong outflows which develop near the ovals as a result of large-scale pressure gradients and magnetospheric forcing imposed by high-latitude ion convection. It is shown that the pole-to-equator circulation of the neutral flow resulting from strong Coriolis torques acting on the equatorward-directed meridional wind, rising motion in the auroral ovals, and subsequent convergence and downwelling motion at the Jovian equator, can regulate the transport of energy outward from the auroral regions to the rest of the planet. We find that such circulation controls the energy budget for the Jovian thermosphere at the entry location of the Galileo ASI probe experiment. Heating is provided by wind transport sources such as adiabatic and hydrodynamic advection for the upper thermosphere (<0.2 μbar), while the thermal conduction becomes an extremely important source of heating between 0.2 μbar and 1 μbar. We also find that the thermal budget for pressures >1 μbar is driven by wind transport processes, and infrared radiation mainly arises from CH_4 and C_2H_2 emissions at 7.8 μm and 12.6 μm, respectively. The transported heat in this region is found to radiate away rapidly causing a net atmospheric imbalance which could be corrected by continuing the simulation for many more planetary rotations.

[40] **Acknowledgments.** We would like to thank A. Ridley and D. Grodent for developing an ionospheric convection model, and B. Foster for his help preparing the JTGCM code to run on the IBM/SP computers. We are also grateful to the National Center for Atmospheric Research (NCAR) for the use of the IBM/SP and SGI supercomputer resources necessary to develop and exercise the JTGCM thermospheric model and its postprocessor. This work is supported by NASA grant NAG 5-11031, NSF grant AST-0300005, and NASA/STScI grant HST-AR-09941.01-A to the University of Michigan.

References

Achilleos, N. S., Miller, J. Tennyson, A. D. Aylward, I. Mueller-Wodarg, and D. Rees (1998), JIM: A time-dependent, three-dimensional model of Jupiter's thermosphere and ionosphere, *J. Geophys. Res.*, *103*, 20,089.

Ajello, J. M., et al. (2001), Spectroscopic evidence for high altitude aurora at Jupiter from Galileo extreme ultraviolet spectrometer and Hopkins ultraviolet telescope observations, *Icarus*, *152*, 151.

Atreya, S. K., T. M. Donahue, and M. Festou (1981), Jupiter—Thermal structure and composition of the upper atmosphere, *Astrophys. J.*, *247*, L43.

Bougher, S. W., S. Engel, R. G. Roble, and B. Foster (1999), Comparative terrestrial planet thermospheres: 2. Solar cycle variation of global structure and winds at equinox, *J. Geophys. Res.*, *104*, 16,591.

Bougher, S. W., J. H. Waite, T. Majeed, and G. R. Gladstone (2005), Jupiter Thermosphere General Circulation Model (JTGCM): Global studies and dynamics driven by auroral and Joule heating, *J. Geophys. Res.*, *110*, E04008, doi:10.1029/2003JE002230.

Clarke, J. T., et al. (1998), Hubble Space Telescope imaging of Jupiter's UV aurora during the Galileo orbiter mission, *J. Geophys. Res.*, *103*, 20,217.

Connerney, J. E. P., M. H. Acuna, N. F. Ness, and T. Satoh (1998), New models of Jupiter's magnetic fields constrained by the Io flux tube footprint, *J. Geophys. Res.*, *103*, 11,929.

Conrath, B. J., P. J. Gierasch, and S. S. Leroy (1990), Temperature and circulation in the stratosphere of the outer planets, *Icarus*, *83*, 255.

Cowley, S. W. H., and E. J. Bunce (2001), Origin of the main auroral oval in Jupiter's coupled magnetosphere-ionosphere system, *Planet. Space Sci.*, *49*, 1067.

Cravens, T. E. (1987), Vibrationally excited molecular hydrogen in the upper atmosphere of Jupiter, *J. Geophys. Res.*, *92*, 11,083.

Dickinson, R. E., E. C. Ridley, and R. G. Roble (1975), Meridional circulation in the thermosphere: I. Equinox conditions, *J. Atmos. Sci.*, *32*, 1737.

Drossart, P., et al. (1989), Detection of H_3^+ on Jupiter, *Nature*, *340*, 539.

Drossart, P., B. Bézard, S. K. Atreya, J. Bishop, J. H. Waite Jr., and D. Boice (1993), Thermal profiles in the auroral regions of Jupiter, *J. Geophys. Res.*, *98*, 18,803.

Eviatar, A., and A. D. Barbosa (1984), Jovian magnetospheric neutral wind and auroral precipitation flux, *J. Geophys. Res.*, *89*, 7393.

Festou, M., et al. (1981), Composition and thermal profile of the Jovian upper atmosphere determined by the Voyager stellar occultation experiments, *J. Geophys. Res.*, *86*, 5715.

Flaser, F. M., et al. (2004), An intense stratospheric jet on Jupiter, *Nature*, *427*, 132.

Gladstone, G. R., M. Allen, and Y. L. Yung (1996), Hydrocarbon photochemistry in the upper atmosphere of Jupiter, *Icarus*, *119*, 1.

Gladstone, G. R., et al. (2002), A pulsating auroral X-ray hot spot on Jupiter, *Nature*, *415*, 1000.

Grodent, D., J. H. Waite Jr., and J.-C. Gerard (2001), A self-consistent model of the Jovian auroral thermal structure, *J. Geophys. Res.*, *106*, 12,933.

Grodent, D., J. T. Clarke, J. Kim, J. H. Waite, and S. W. H. Cowley (2003), Jupiter's main auroral oval observed with HST-STIS, *J. Geophys. Res.*, *108*(A11), 1389, doi:10.1029/2003JA009921.

Hickey, M. P., R. L. Walterscheid, and G. Schubert (2000), Gravity wave heating and cooling in Jupiter's thermosphere, *Icarus*, *148*, 266.

Hill, T. W. (2001), The Jovian auroral oval, *J. Geophys. Res.*, *106*, 8101.

Hubbard, W. B., V. Hammerle, C. C. Porco, G. H. Rieke, and M. J. Rieke (1995), The occultation of SAO 78505 by Jupiter, *Icarus*, *113*, 103.

Hunten, D. M., and A. J. Dessler (1997), Soft electrons as a possible heat source for Jupiter's thermosphere, *Planet. Space Sci.*, *25*, 817.

Lam, H. A., et al. (1997), A baseline spectroscopic study of the infrared auroras of Jupiter, *Icarus*, *127*, 379.

Liu, W., and A. Dalgarno (1996), The ultraviolet spectrum of the Jovian dayglow, *Astrophys. J.*, *462*, 502.

Majeed, T., and J. C. McConnell (1991), The upper ionosphere of Jupiter and Saturn, *Planet. Space Sci.*, *39*, 1715.

Majeed, T., J. C. McConnell, and G. R. Gladstone (1999), A model analysis of Galileo electron densities on Jupiter, *Geophys. Res. Lett.*, *26*, 2335.

Majeed, T., J. H. Waite, S. W. Bougher, R. V. Yelle, G. R. Gladstone, J. C. McConnell, and A. Bhardwaj (2004), The ionospheres-thermospheres of the giant planets, *Adv. Space Res.*, *33*, 197.

Marten, A., C. DeBergh, T. Owen, D. Gautier, J. P. Maillard, P. Drossart, B. L. Lutz, and G. S. Orton (1994), Four micron high-resolution spectra of Jupiter in the North Equatorial Belt: H_3^+ emissions and $^{12}C/^{13}C$ ratio, *Planet. Space Sci.*, *42*, 391.

Matcheva, K. I., and D. F. Strobel (1999), Heating of Jupiter's thermosphere by dissipation of gravity waves due to molecular viscosity and heat conduction, *Icarus*, *140*, 328.

Matsushita, S., J. D. Tarpley, and W. H. Campbell (1973), IMF sector structure effects on the quiet geomagnetic field, *Radio Sci.*, *8*, 963.

Maurellis, A. N., and T. E. Cravens (2001), Ionospheric effects of comet Shoemaker-Levy 9 impacts with Jupiter, *Icarus*, *154*, 350.

Maurellis, A. N., T. E. Cravens, G. R. Gladstone, J. H. Waite, and L. W. Acton (2000), Jovian X-ray emission from solar X-ray scattering, *Geophys. Res. Lett.*, *27*, 1339.

Miller, S., N. Achilleos, G. E. Ballester, H. A. Lam, J. Tennyson, T. R. Geballe, and L. M. Trafton (1997), Mid-to-low latitude H_3^+ emission from Jupiter, *Icarus*, *130*, 57.

Millward, G. H., S. Miller, A. D. Aylward, I. C. F. Muller-Wodarg, and N. Achilles (2002), Thermospheric General Circulation Models for the giant planets: The Jupiter case, in *Atmospheres in the Solar System: Comparative Aeronomy*, *Geophys. Monogr. Ser.*, vol. 130, edited by M. Mendillo, A. Nagy, and J. H. Waite, pp. 289–298, AGU, Washington, D. C.

Moses, J. I., et al. (2004), The stratosphere of Jupiter, in *Jupiter: The Planet, Satellites and Magnetosphere*, edited by F. Bagenal, T. Dowling, and W. McKinnon, pp. 129–157, Cambridge Univ. Press, New York.

Niemann, H. B., et al. (1996), The Galileo Probe Mass Spectrometer: Composition of Jupiter's atmosphere, *Science*, *272*, 846.

Raynaud, E., et al. (2004), Spectro-imaging observations of Jupiter's 2-micron auroral emission: I. H_3^+ distribution and temperature, *Icarus*, *171*, 133.

Richmond, A. D., E. C. Ridley, and R. G. Roble (1992), A thermosphere/ionosphere general circulation model with coupled electrodynamics, *Geophys. Res. Lett.*, *19*, 601.

Roble, R. G., and E. C. Ridley (1987), An auroral model for the NCAR thermospheric general circulation model (TGCM), *Ann. Geophys. Ser. A*, *5*, 369.

Roble, R. G., and E. C. Ridley (1994), A thermosphere-ionosphere-magnetosphere-electrodynamics circulation model (TIME-GCM): Equinox solar minimum simulations (30–500 km), *Geophys. Res. Lett.*, *21*, 417.

Roble, R. G., E. C. Ridley, A. D. Richmond, and R. E. Dickinson (1988), A coupled thermospheric-ionospheric general circulation model, *Geophys. Res. Lett.*, *15*, 1325.

Sieff, A., D. B. Kirk, T. C. D. Knight, R. E. Young, J. D. Mihalov, L. A. Young, F. S. Milos, G. Schubert, R. C. Blanchard, and D. Atkinson (1998), Thermal structure of Jupiter's atmosphere near the edge of a 5-μm hot spot in the north equatorial belt, *J. Geophys. Res.*, *103*, 22,857.

Sommeria, J., L. Ben-Jaffel, and R. Prange (1995), On the existence of supersonic jets in the upper atmosphere of Jupiter, *Icarus*, *119*, 2.

Strobel, D. F., and G. R. Smith (1973), On the temperature of the Jovian thermosphere, *J. Atmos. Sci.*, *30*, 489.

Waite, J. H., Jr., T. E. Cravens, J. U. Kozyra, A. F. Nagy, S. K. Atreya, and R. H. Chen (1983), Electron precipitation and related aeronomy of the Jovian thermosphere and ionosphere, *J. Geophys. Res.*, *88*, 6143.

Waite, J. H., et al. (1997), Equatorial X-ray emissions: Implications of Jupiter's high exospheric temperatures, *Science*, *276*, 104.

Yelle, R. V., and S. Miller (2004), Jupiter's thermosphere and ionosphere, in *Jupiter: The Planet, Satellites and Magnetosphere*, edited by F. Bagenal, T. Dowling, and W. McKinnon, pp. 185–218, Cambridge Univ. Press, New York.

Yelle, R. V., L. A. Young, R. J. Vervack, R. Young, L. Pfister, and B. R. Sandel (1996), Structure of Jupiter's upper atmosphere: Prediction for Galileo, *J. Geophys. Res.*, *101*, 2149.

Yelle, R. V., C. A. Griffith, and L. A. Young (2001), Structure of the Jovian stratosphere at the Galileo probe entry site, *Icarus*, *152*, 331.

Young, L. A., R. V. Yelle, R. Young, A. Sieff, and D. B. Kirk (1997), Gravity waves in Jupiter's thermosphere, *Science*, *276*, 108.

Young, L. A., R. V. Yelle, R. Young, A. Sieff, and D. B. Kirk (2005), Gravity waves in Jupiter's stratosphere, as measured by the Galileo ASI experiment, *Icarus*, *173*, 185.

S. W. Bougher and J. H. Waite Jr., Space Physics Research Laboratory, University of Michigan, Ann Arbor, MI 48109-2143, USA. (bougher@umich.edu; hunterw@umich.edu)

G. R. Gladstone, Southwest Research Institute, San Antonio, TX 78228-0510, USA. (randy@whistler.space.swri.edu)

T. Majeed, Department of Physics, American University of Sharjah, P.O. Box 26666, Sharjah, UAE. (tmajeed@aus.edu)